Supplementary Materials

Deformation and breakup of a ferrofluid compound droplet migrating in a microchannel under a magnetic field: A phase-field-based multiple-relaxation time lattice Boltzmann study

Parham Poureslami[1], Mohammad majidi[2], Javad Ranjbar Kermani[1], and Mohamad Ali Bijarchi[1*]

[1]Department of Mechanical Engineering, Sharif University of Technology, Tehran, Iran

[2]Brown University, School of Engineering, Providence, RI, US

[*]Author to whom correspondence should be addressed: bijarchi@sharif.edu

Fig. S1 illustrates the 2-dimensional 9-discrete velocity (D2Q9) model utilized in the lattice-Boltzmann formulation for the flow field in this research.

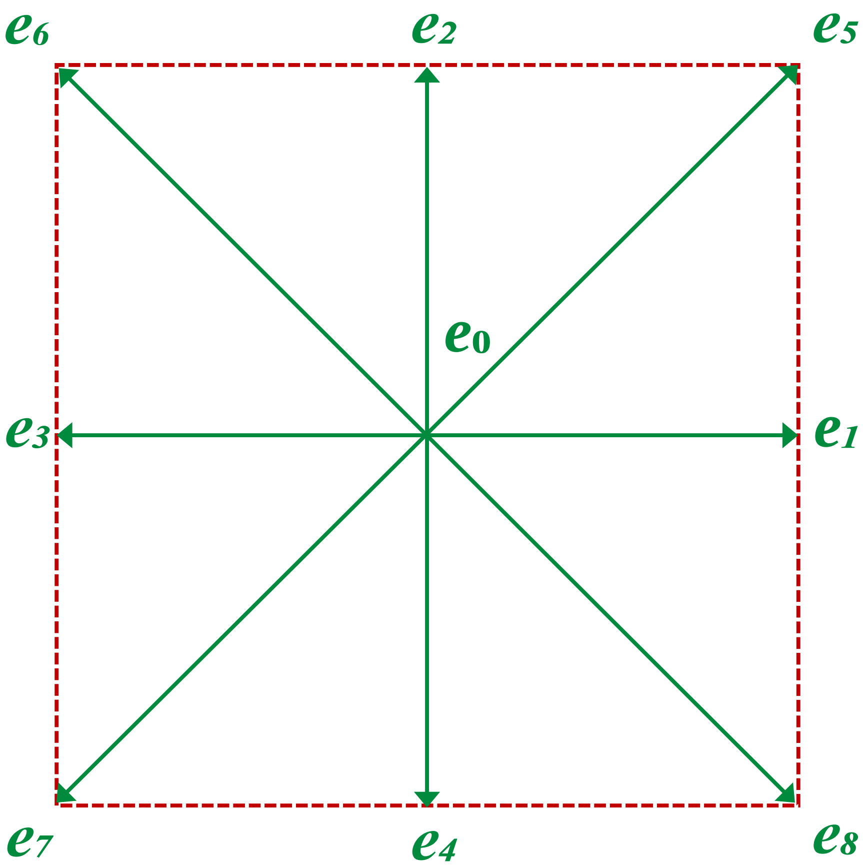

Fig S1: The D2Q9 lattice structure.

Fig. S2 compares the grid convergence results for three distinct grids of 100×600, 150×900, and 200×1200 for distinguished regimes achieved by varying the magnetic Bond number from 0 to 8 and the Capillary number from 0.05 to 0.30.

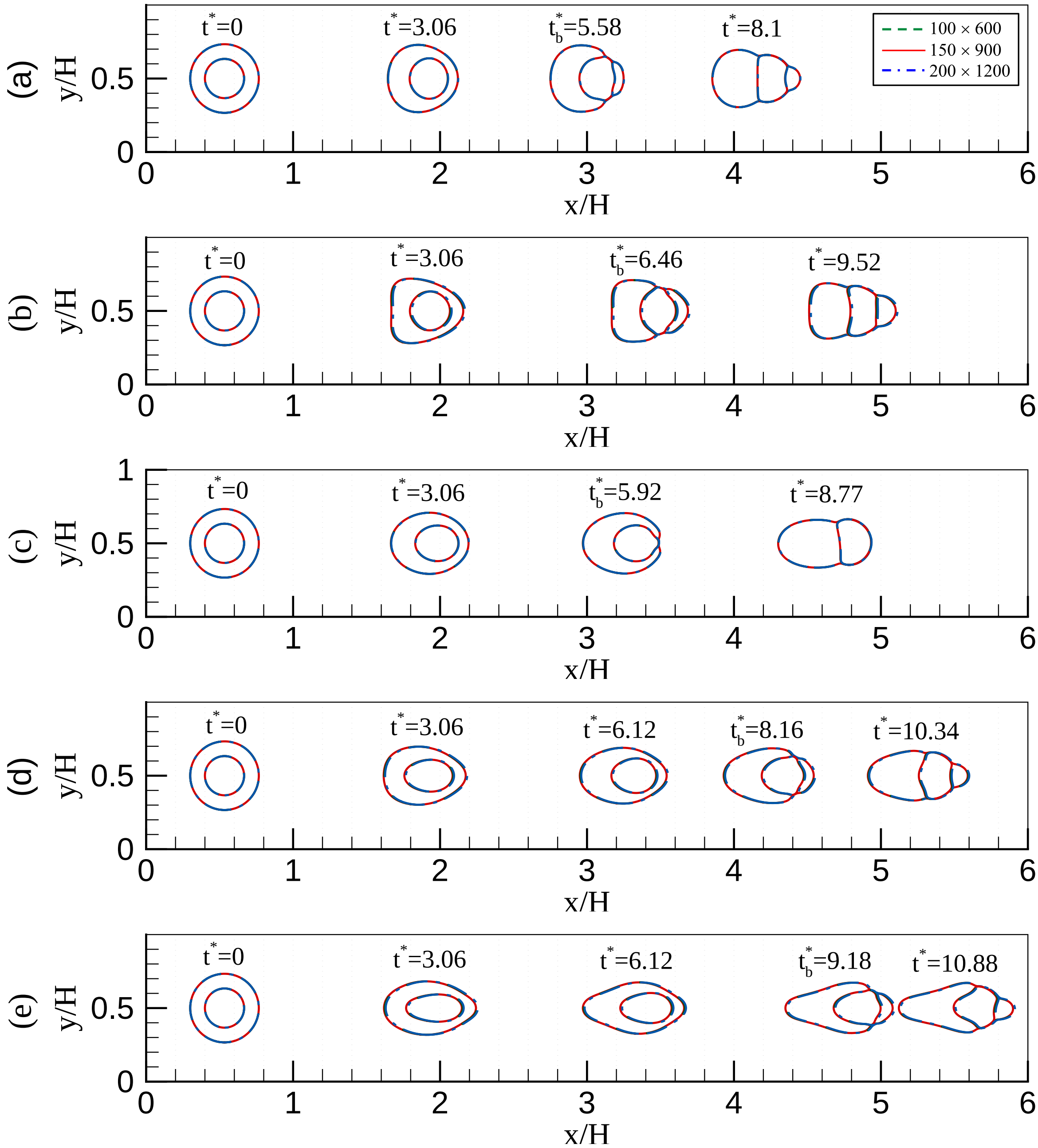

Fig S2: Comparison of the results obtained by three different grid resolutions (100×600, 150×900, and 200×1200) to explore the grid convergence for five distinguished regimes observed during the migration of a ferrofluid compound droplet in a microchannel under the influence of a uniform external magnetic field. The shell is presumed to be ferrofluid and the magnetic field is applied along $\alpha = 0°$; (a) semi-spherical regime ($\mathrm{Bo}_m = 0$, $\mathrm{Ca} = 0.05$), (b) triangular-like regime ($\mathrm{Bo}_m = 1$, $\mathrm{Ca} = 0.25$), (c) egg-like-type 1 regime ($\mathrm{Bo}_m = 2$, $\mathrm{Ca} = 0.05$), (d) egg-like-type 2 regime ($\mathrm{Bo}_m = 4$, $\mathrm{Ca} = 0.20$), and (e) tadpole-like regime ($\mathrm{Bo}_m = 7$, $\mathrm{Ca} = 0.25$). Dashed lines, solid lines, and dashed-dotted lines are representative of 100×600, 150×900, and 200×1200 grids, respectively. t_b^* denotes the dimensionless breakup time.

1 A validation case: single droplet migration through microchannel in a fully developed flow

Hereby, we propose a new validation to evaluate the accuracy of the implemented boundary conditions by modeling the migration of a single droplet in a microchannel under fully developed flow in the absence of the magnetic field ($\mathrm{Bo}_m = 0$). We adopted the same settings as Wang et al. (Wang et al., 2020) so that the results may be quantitatively compared.

At the inlet, as discussed in the manuscript, the Zou and He (Zou and He, 1997) velocity condition with parabolic profile is imposed:

$$\begin{cases} u = 4u_{avg}\dfrac{y}{H}\left(1-\dfrac{y}{H}\right) \\ v = 0 \end{cases} \tag{1}$$

where u and v denote the velocity along the x- and y-directions, respectively, and H symbolizes the channel height. u_{avg} represents the average velocity. At the outlet, a convective boundary condition (CBC) is applied, while no-slip conditions are imposed on the sidewalls. The viscosities of both the droplet and the ambient fluid are set to 0.167, and the surface tension is 0.005.

Initially, having the diameter of $D = 40$, the droplet is positioned at (60, 49.5) in a computational domain of size $L \times H = 399 \times 99$. The initial configuration is illustrated in Fig. S3 (a). Simulations are conducted for two distinct values of $u_{avg} = 1.5 \times 10^{-3}$ and $u_{avg} = 3.0 \times 10^{-4}$. The time evolution of the dimensionless leftmost droplet position (X_D^*), $X_D^* = \dfrac{X_D}{D}$, is compared with the results of Wang et al. (Wang et al., 2020), as shown in Fig. S3 (b) and (c). The average relative errors are 3.14% and 3.26% for $u_{avg} = 1.5 \times 10^{-3}$ and $u_{avg} = 3.0 \times 10^{-4}$, respectively, demonstrating the favorable accuracy of the solver. Moreover, Fig. S3 indicates that X_D^* grows linearly with time, consistent with Wang et al. (Wang et al., 2020).

2 Sensitivity of the results to the mobility parameter M

Fig. S4 quantifies the impact of mobility parameter $M \in \{0.05, 0.075, 0.10\}$ on the single and compound droplet motion and deformation. Specifically, Fig. S4 (a) compares the leftmost position of a single droplet versus time during its movement in the microchannel with the results of Wang et al. (Wang et al., 2020) at $u_{avg} = 1.5 \times 10^{-3}$. Evidently, altering the mobility parameters does not significantly affect X_D^*. Fig. S4 (b) reveals the single droplets interface at $t^* = 3.75$ for the considered values of M, where all interfaces collapse onto a single curve. Additionally, Fig. S4 (c) depicts the migration process of FCD in the microchannel under the simultaneous presence of pressure-driven flow and magnetic field when $\mathrm{Bo}_m = 4$ and $\mathrm{Ca} = 0.15$ for different values of M. Overall, Fig. S4 suggests that for the configuration and parameter range examined, varying the mobility parameter does not lead to appreciable differences in key physical quantities.

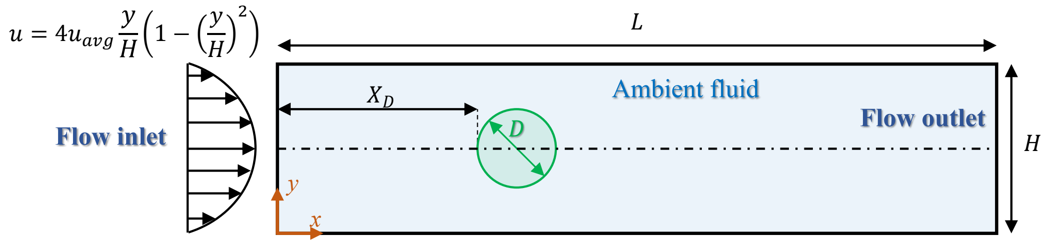

(a)

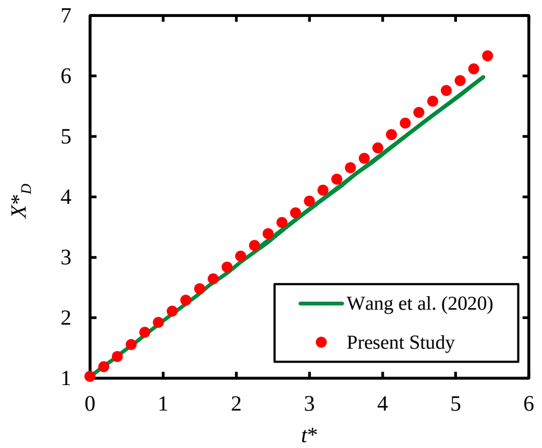

(b) $u_{avg} = 1.5 \times 10^{-3}$

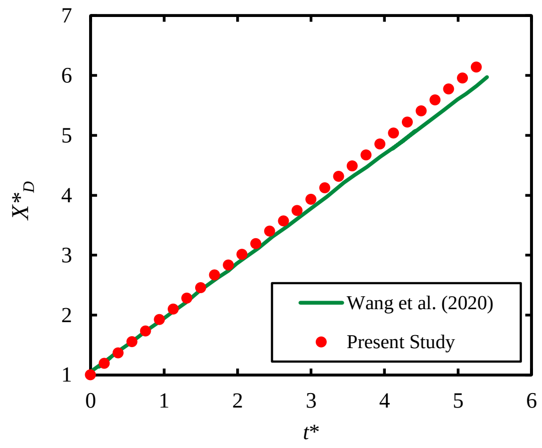

(c) $u_{avg} = 3.0 \times 10^{-4}$

Fig S3: Validation of droplet migration in a microchannel under the fully developed flow; (a) schematic of the initial configuration, (b) and (c) comparison of X_d^* as a function of dimensionless time t^*, where $t^* = \frac{tu_{avg}}{D}$, with those obtained by Wang et al. (Wang et al., 2020) for two distinct values of u_{avg}. X_D represents the droplets leftmost position relative to the inlet ($x = 0$), normalized by $X_D^* = \frac{X_D}{D}$.

3 Wall confinement effect

In this section, we examine the effects of confinement ratio, defined as $\lambda = \frac{2r_2}{H}$, on the FCD deformation. Specifically, by keeping the Ca, Bo_m, and inner and outer droplet radii constant, we examine three different channel heights corresponding to confinement ratios of $\lambda = 0.28$, $\lambda = 0.47$, and $\lambda = 0.74$, respectively. Fig. S5 shows the impact of the confinement ratio on the FCD at $\text{Bo}_m = 0$, Ca = 0.15, $\nu_r = 1$, and $\rho_r = 1$. The interface shape is analyzed when the FCD leftmost position reaches the same location ($\frac{x}{H} \approx 1.90$). Evidently, as the channel height decreases (i.e., the confinement ratio increases), the deformation of the FCD becomes more pronounced due to enhanced wall shear stress and confinement effects. Moreover, as λ increases, the rear side of the outer droplet stretches vertically, which is consistent with the findings of Che et al. (Che et al., 2018). Table S1 compares the deformation of inner and outer droplets for different λ values. The reported results correspond to the moment depicted in Fig S5. Regarding Table S1, confining the channel significantly affects FCD deformation, with a more pronounced impact on the shell.

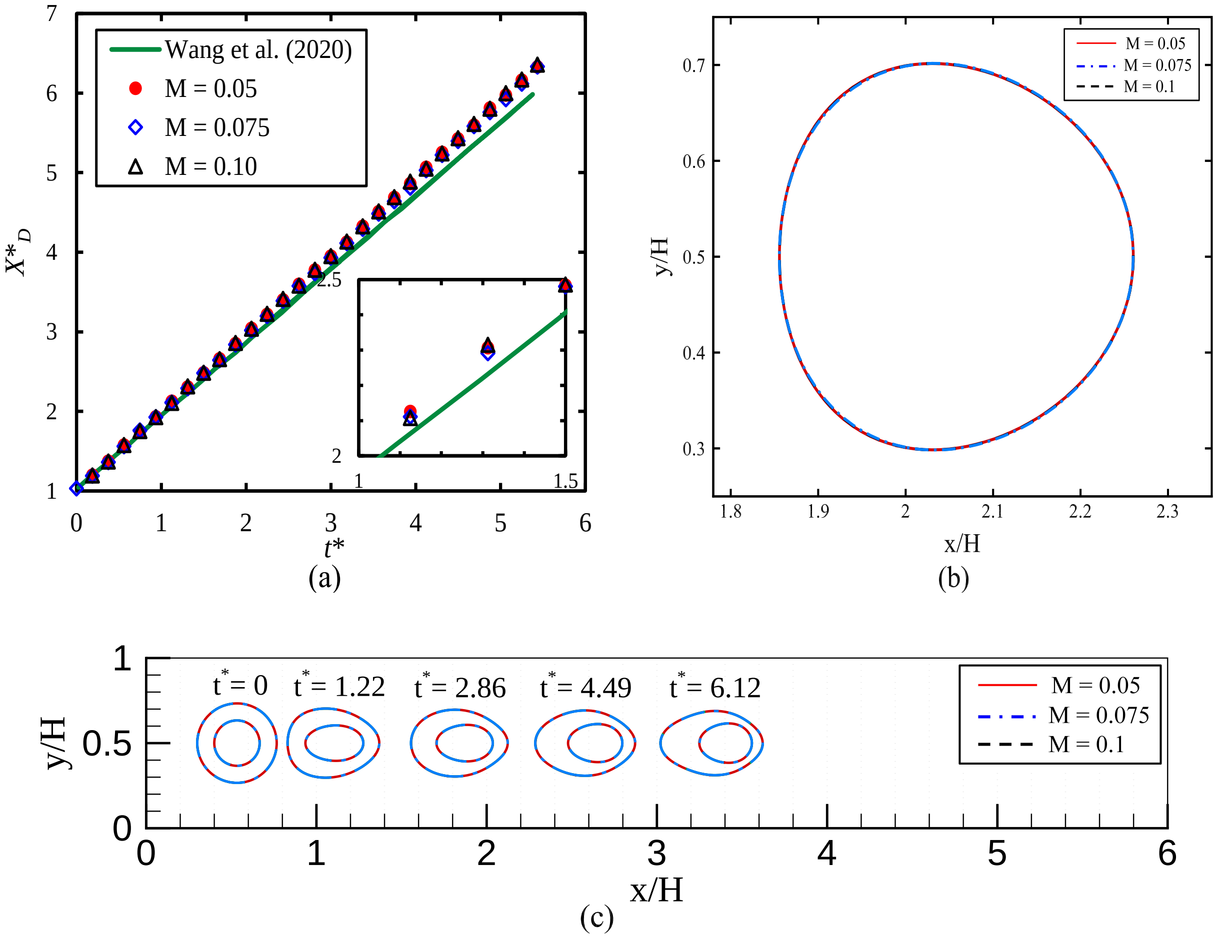

Fig S4: Quantifying the effect of mobility M on the single and compound droplet motion and deformation; (a) comparison of X_d^* as a function of dimensionless time $t^* = \dfrac{tu_{avg}}{D}$, with the results of Wang et al. (Wang et al., 2020) for three distinct values of M. The inset magnifies the trivial differences in results; (b) single droplet interface during its migration in the microchannel under the sole presence of fully developed flow when $u_{avg} = 1.5 \times 10^{-3}$ at $t^* = 3.75$, and (c) traversing process of FCD under the concurrent influence of fully developed flow and UEMF when $\mathrm{Bo}_m = 4$ and $\mathrm{Ca} = 0.15$.

Table S1: Effect of wall confinement ratio, λ, on the deformation of inner and outer droplets when $\mathrm{Bo}_m = 0$, $\mathrm{Ca} = 0.15$, and the outer droplet is ferrofluid. The reported values correspond to the moment shown in Fig. S5.

λ	T_o	T_i
0.74	-0.075	0.06
0.47	-0.037	0.065
0.28	-0.011	0.028

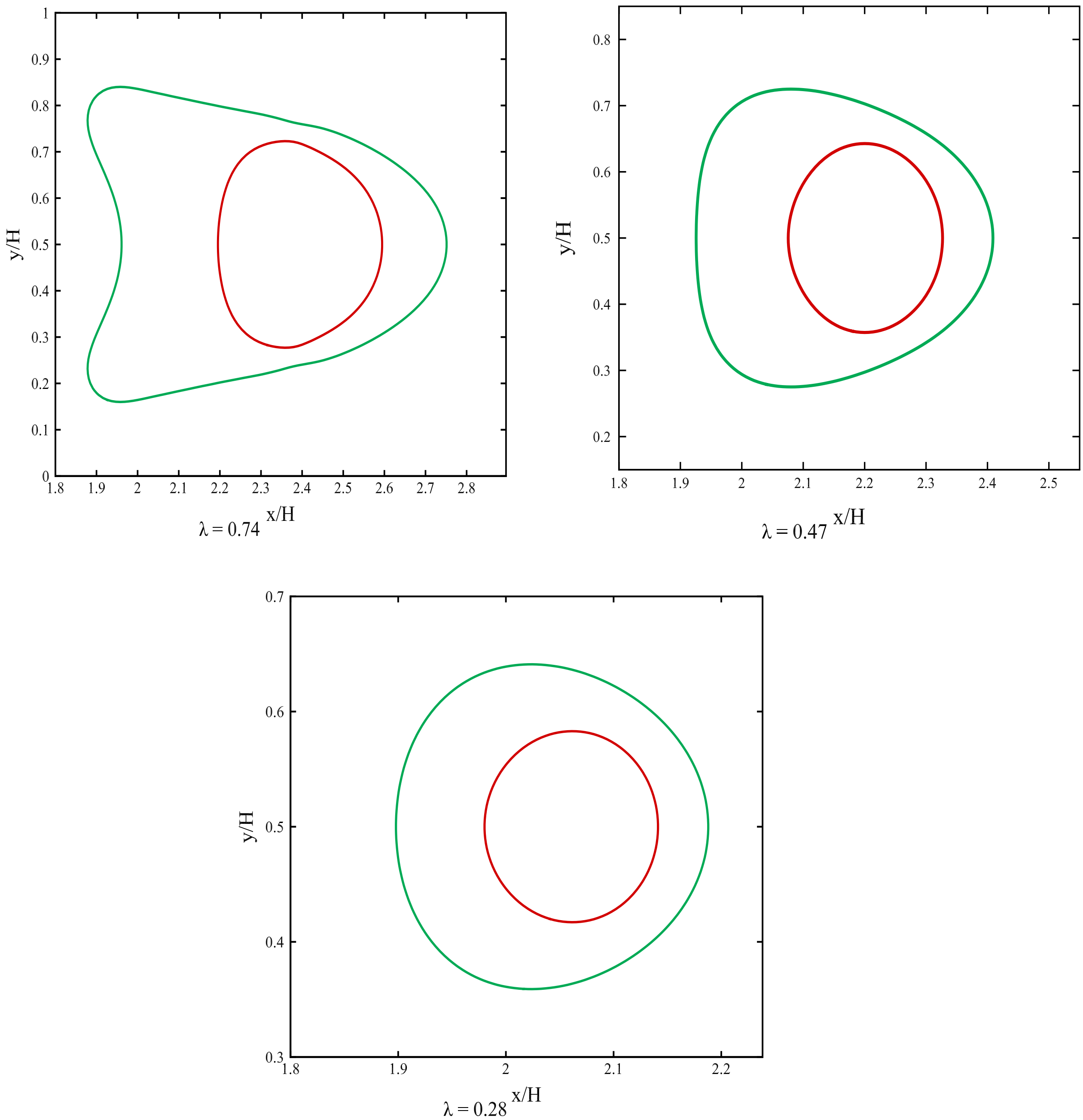

Fig S5: Effects of wall confinement (λ) on the FCD deformation when Ca = 0.15, Bo_m = 0, and outer droplet is ferrofluid.

4 A case study: deformation and breakup of O/W/O and W/O/W Configurations

As a case study, to assess the ferrofluid compound droplet (FCD) hydrodynamics under a real thermophysical condition, two conventional configurations of compound droplets are considered, which are oil-in-water-in-oil (O/W/O) and water-in-oil-in-water (W/O/W) configurations (van der Graaf et al., 2005). The thermophysical properties of the adopted configurations are given in Table S2 (Mohseni et al., 2024).

Table S2: Properties of W/O/W and O/W/O configurations (Mohseni et al., 2024).

Configuration	Inner droplet	Outer droplet	Ambient fluid	$\rho_r = \frac{\rho_1}{\rho_2}$	$\nu_r = \frac{\nu_1}{\nu_2}$
O/W/O	Olive oil	Water-based Ferrofluid	Olive oil	0.787	20.04
W/O/W	Water	Oil-based Ferrofluid (EMG 901)	Water	0.698	0.129

Fig. S6 demonstrates the traversing process of a ferrofluid compound droplet (FCD) under the uniform external magnetic field (UEMF) at four distinct values of the magnetic Bond numbers (Bo_m) for O/W/O configuration when Ca = 1 and the shell is supposed to be ferrofluid. Given Fig. S6, at $\mathrm{Bo}_m = 0$, in which no magnetic force is applied, the breakup occurs promptly at $t_b^* = 3.88$, which emanates from a meager shell viscosity, curtailing the force the core requires to move inside the shell, which in turn, gives rise to a swift rupture. On the other hand, once the magnetic field is imposed, the breakup phenomenon is retarded conspicuously, which may be justified by two paramount reasons: 1) both the magnetic and viscous force strive to stretch the shell in the horizontal direction, engendering an oblate-like shape. Accordingly, the core is given more space so that it can move further inside the shell prior to rupture. 2) Induced by the magnetic force, the striking horizontal elongation of the shell reduces the drag force exerted on the outer droplet, postponing the breakup. To put it another way, in view of the smaller drag force applied to the shell, the FCD can further transport in the channel in advance of the breakup. Additionally, augmenting the Bo_m number suppresses the inner droplet vertical elongation at the rupture moment, decreasing the height at which the core touches the shell interface (y_b^*).

Table S3: L_b^*, t_b^*, and y_b^* for O/W/O configuration at Ca = 1 at various magnetic Bond numbers. The shell is presumed to be ferrofluid, and the UEMF is exerted at $\alpha = 0°$.

Bo_m	L_b^*	t_b^*	y_b^*
0	2.39	3.88	0.165
1	2.74	4.49	0.15
2	2.99	4.90	0.128
4	3.29	5.31	0.1
8	3.69	5.97	0.088

Table S3 summarizes the dimensionless breakup length (L_b^*), dimensionless breakup time (t_b^*), and nondimensional rupture height with respect to the channel center line (y_b^*) for O/W/O configuration at Ca = 1. As can be seen, by raising the Bom number from 0 to 4, one may decelerate the breakup by 36.9%.

Fig. S7 indicates the migration of an FCD with W/O/W configuration in a microchannel over time under the UEMF for disparate values of Bom numbers when Ca = 1 and the shell is ferrofluid. Interestingly, breakup happens at neither shown Bo_m numbers for the W/O/W configuration, which is instigated by the drastic shell viscosity. Actually, as it is discussed in the manuscript, the greater the shell viscosity, the more the shell is analogous to the solid, which slows down the core movement inside the shell, remarkably retarding the rupture

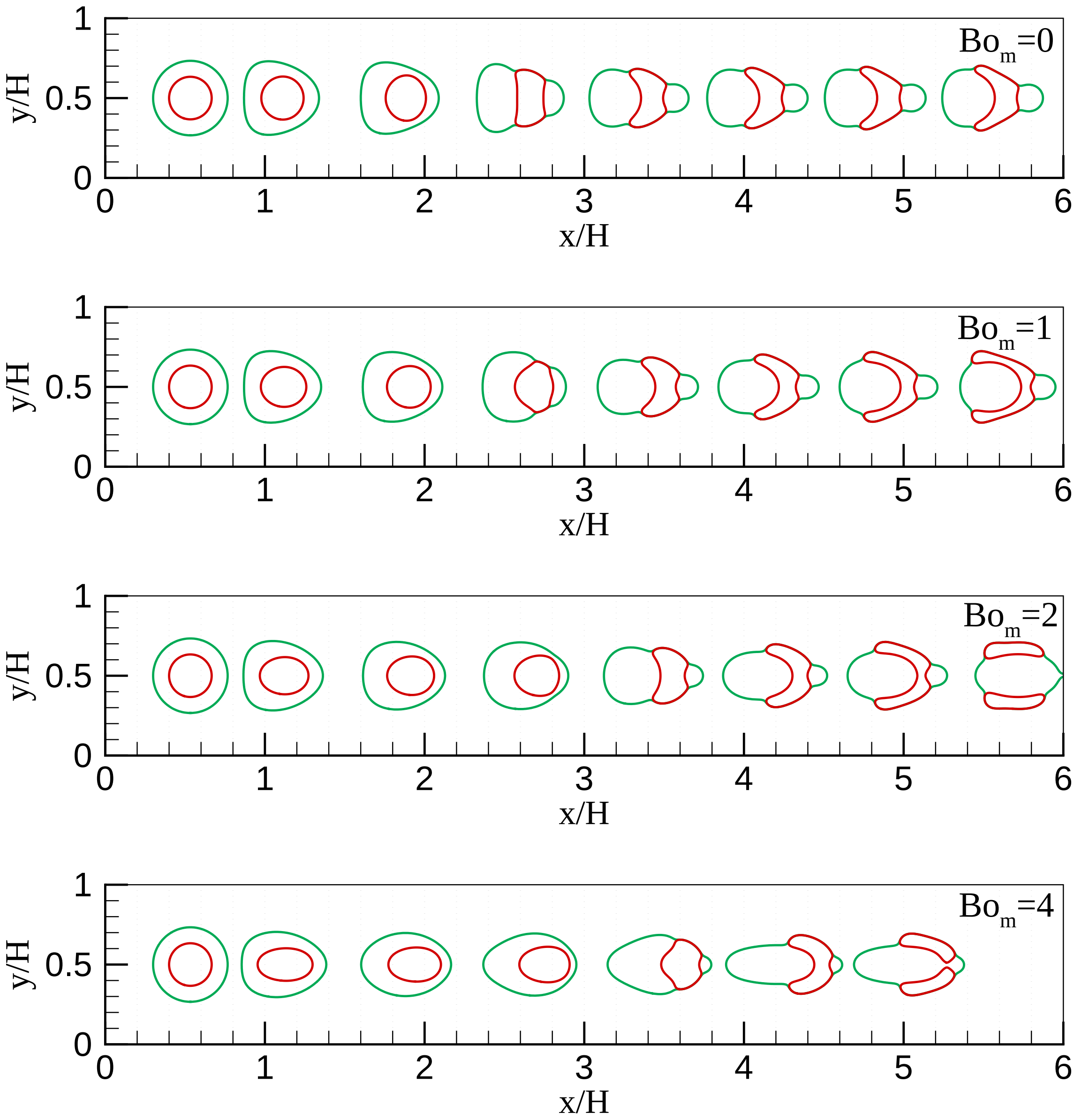

Fig S6: The migration of an FCD with O/W/O configuration inside a microchannel from the initial point to the outlet over time for various magnetic Bond numbers at $\alpha = 0°$ and Ca = 1 when the shell is ferrofluid. From left to right: $t^* = 0$, 1.22, 2.86, 4.49, 6.12, 7.75, 9.39 and 11.02.

incident such that the breakup does not happen at $x/H < 6$. Regarding the FCD morphology during the traversing, when the magnetic force is low, the conspicuous drag force flattens the shells rear side, engendering a triangular-like shell. On the contrary, as the magnetic force is intensified, the shell is elongated horizontally from both sides, which conveys that the shell reaches an ellipsoid configuration (See Fig. S7 at $\mathrm{Bo}_m = 4$)

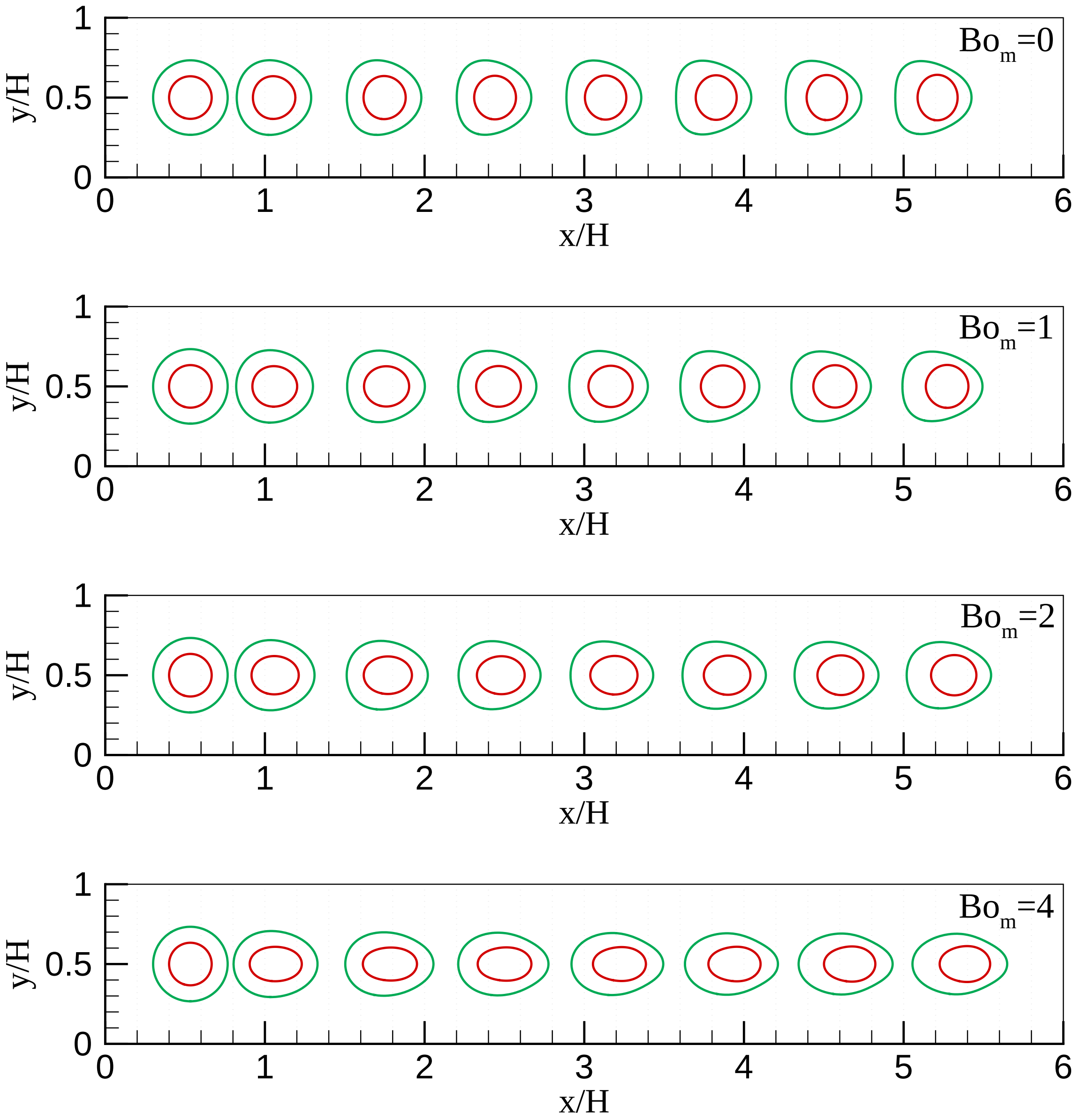

Fig S7: The migration of an FCD with W/O/W configuration inside a microchannel from the initial point to the outlet over time for various magnetic Bond numbers at $\alpha = 0°$ and Ca = 1 when the shell is ferrofluid. From left to right: $t^* = 0, 1.22, 2.86, 4.49, 6.12, 7.75, 9.39$ and 11.02.

References

Zhizhao Che, Yit Fatt Yap, and Tianyou Wang. Flow structure of compound droplets moving in microchannels. *Physics of Fluids*, 30(1), 2018.

Alireza Mohseni, Ali Abbas Azimi, and Mohamad Ali Bijarchi. Formation of magnetic double emulsions under steady and variable magnetic fields from a 3d-printed coaxial capillary device. *Analytica Chimica Acta*, 1309:342573, 2024.

Schroen van der Graaf, CGPH Schroën, and RM Boom. Preparation of double emulsions by membrane emulsificationa review. *Journal of Membrane Science*, 251(1-2):7–15, 2005.

Ningning Wang, Ciro Semprebon, Haihu Liu, Chuhua Zhang, and Halim Kusumaatmaja. Modelling double emulsion formation in planar flow-focusing microchannels. *Journal of Fluid Mechanics*, 895:A22, 2020.

Qisu Zou and Xiaoyi He. On pressure and velocity boundary conditions for the lattice boltzmann bgk model. *Physics of fluids*, 9(6):1591–1598, 1997.